



Cite this: DOI: 10.1039/d0pp00140f

Unusual absence of FRET in triazole bridged coumarin–hydroxyquinoline, an active sensor for Hg²⁺ detection†

Surajit Mondal,^a Niladri Patra,^{*a} Hari Pada Nayek,^{id}^a Sumit K. Hira,^{id}^b Soumit Chatterjee^{id}^{*a} and Swapan Dey^{id}^{*a}

A triazole-bridged coumarin conjugated quinoline sensor has been 'click'-synthesized by Cu(I) catalyzed Huisgen cycloaddition, and it exhibited high selectivity for toxic Hg²⁺. Surprisingly, no evidence of energy transfer from the quinoline moiety to coumarin has been found, substantiated by time-resolved fluorescence study. The possible binding mode of this sensor to Hg²⁺ has been established *via* NMR study, steady-state and time-resolved fluorescence spectroscopy, which is further supported by TDDFT calculations. The sensor has been found to be cell membrane permeable and non-toxic, and hence is suitable for intracellular Hg²⁺ detection.

Received 10th April 2020,
Accepted 8th July 2020

DOI: 10.1039/d0pp00140f

rsc.li/pps

Introduction

Mercury contamination through the cell membrane creates severe harmful effects on human health.^{1,2} Organic methyl mercury (CH₃Hg⁺), generated from both elemental and ionic mercury by bacterial action, causes several adverse effects to the central nervous system, endocrine system, kidneys, skin and DNA.^{3–7} Mercury ion is also highly responsible for environmental pollution. Therefore, quantitative recognition of elemental or ionic mercury is imperative in the current scenario. A variety of techniques like atomic absorption spectrometry (AAS) and inductively coupled plasma-mass spectrometry (ICPMS)^{8,9} have been used for the qualitative detection of Hg²⁺ in the recent past. In addition to this, a supramolecular gel-based sensor,^{10,11} especially Hg²⁺ promoted sol-gel transformation, has been considerably used. Yet this strategy has suffered from selectivity issues.^{12,13} However, these processes are expensive, time-consuming and require specific technical skills for machine operation and are only limited to scientific research.

On the other hand, the use of suitable fluorophores for the detection of Hg²⁺ is beneficial due to their sensitivity, simplicity and low cost.^{14–16}

The basis of fluorometric detection of metal ions lies on the nature of metal ion binding with the fluorophore, resulting in the enhancement or quenching of the quantum yield of the latter by virtue of various associated photophysical processes. In general, the possible phenomena related to these kinds of adducts can be fluorescence resonance energy transfer (FRET), photoinduced electron transfer (PET), through bond energy transfer (TBET) *etc.* Coumarin derivatives have been widely used for designing sensory systems due to their sensible photophysical properties with a large Stokes shift and visible emission wavelength.^{17–19} They are frequently used in the development of chemosensors and chemodosimeters due to their high solubility in polar protic solvents.^{20–25} In addition, 8-hydroxyquinoline (8-HQ) has also been extensively used in designing chemosensors for the detection of metal ions such as Cu²⁺,²⁶ Cd²⁺,²⁷ Mg²⁺,²⁸ Zn²⁺,^{29,30} Al³⁺,³¹ and Hg²⁺,³² due to their photostability and strong complexation ability. For example, Ho and co-workers have reported three coumarin based triazole fluorophores for the detection of Hg²⁺.³³ A conformationally constrained quinoline coupled coumarin fluorophore moiety has also been reported for the selective detection of Al³⁺.^{34,35} However, in all these cases, the triazole was not directly attached to coumarin. Therefore in continuation of our recent development on designing chemosensors,^{36–40} we present, herein, the synthesis and characterization of a three triazole cross-linked simple chemosensor (**R1**) which exhibits a large Stokes shift and quick response to Hg²⁺ with high sensitivity and excellent selectivity.

^aDepartment of Chemistry, Indian Institute of Technology (Indian School of Mines), Dhanbad, Jharkhand, India. E-mail: swapan@iitism.ac.in

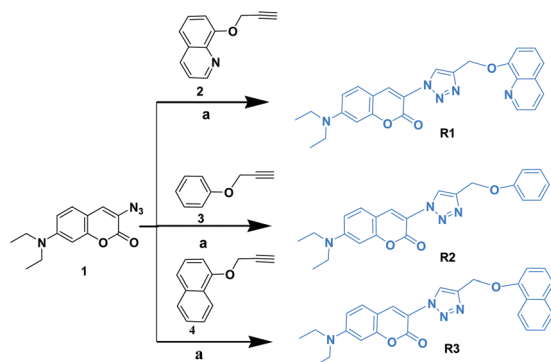
^bDepartment of Zoology, The University of Burdwan, Burdwan, West Bengal 713104, India

† Electronic supplementary information (ESI) available: Characterisation data of all compounds, ESI mass and FT-IR of complex, binding constant calculation table, LOD calculation, reversibility test and bar diagram, synthetic procedure of coumarin amine. CCDC 1944133, 1904920 and 1904921. For ESI and crystallographic data in CIF or other electronic format see DOI: 10.1039/d0pp00140f

Results and discussion

Synthesis of R1, R2 and R3

All three sensors (**R1**, **R2** and **R3**), in which a 1,2,3-triazolyl ring is flanked by coumarin and 8-hydroxyquinoline (8-HQ) (for **R1**), phenyl (**R2**) and naphthalene (**R3**) moieties respectively, had been synthesized based on the synthetic variations of the “click” reaction. The excellent complexation properties of the resulting electron-rich 1,2,3-triazolyl moiety,^{41–45} facilitated by Cu(I)-catalyzed 1,3-dipolar cycloaddition of terminal alkynes and azides. Coumarin azide has been synthesized following a known procedure and used as a precursor for the syntheses of three different compounds **R1**, **R2** and **R3**.⁴⁶ The synthetic routes of the sensors are shown in Scheme 1 and the detailed procedures are given in the Experimental section. The single crystals of the sensors were generated from a different proportion of the ethyl acetate–pet ether mixture. Single-crystal X-Ray studies revealed that both **R1** and **R3** were triclinic systems with the $P\bar{1}$ space group, while **R2** was monoclinic with the $P2_1/c$ space group. The ORTEP diagram (Fig. 1) confirmed that the 8-HQ (**R1**), phenyl (**R2**) and naphthalene moieties (**R3**) were oriented almost perpendicular to that of the



Scheme 1 Reagents and conditions:(a) CuSO_4 , sodium ascorbate, DCM : EtOH (1 : 1), rt, 12 h.

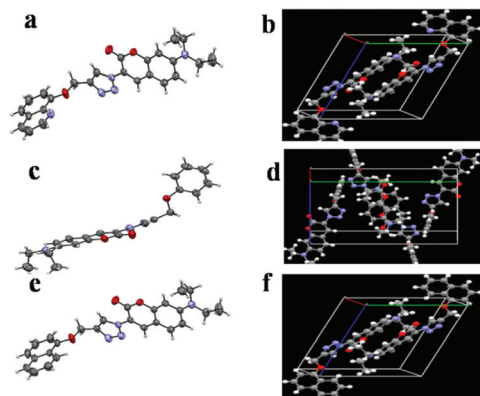


Fig. 1 Single crystal structure of **R1** (a) ORTEP along b and (b) packing diagram along a , **R2** (c) ORTEP and (d) packing diagram along a and of **R3** (e) ORTEP and (f) packing diagram along a (30% probability).

coumarin moiety with torsional angles of 11.15 (1°), 6.72 (1°) and 11.23 (2°), respectively and for all the compounds the triazole rings were found to be coplanar to coumarin.

Steady-state spectroscopy

The solutions of all three sensors (**R1**, **R2** and **R3**) were prepared in ethanol and were found to exhibit green fluorescence upon long-wavelength UV exposure. Upon the addition of Hg^{2+} , the fluorescence of **R1** was dramatically quenched. Other metal ions such as Li^+ , Mg^{2+} , Al^{3+} , Fe^{3+} , Co^{2+} , Ni^{2+} , Zn^{2+} , Ag^+ , Cd^{2+} , Ba^{2+} , and Pb^{2+} did not show any remarkable response (Fig. 3). However, with Cu^{2+} , the emission intensity was quenched, but, to a much lesser extent than Hg^{2+} . The complete absorption and emission studies are discussed in the following paragraphs. **R2** and **R3**, on the other hand, did not show any detectable changes upon the addition of Hg^{2+} (Fig. S1, ESI[†]). **R1** (3.4×10^{-5} M in EtOH) displayed an absorption maximum at 412 nm and another strong benzenoid band at around 250 nm. After the gradual addition of Hg^{2+} up to 10.0 equivalents, the peak position of the 412 nm band remained unchanged. Still, the optical density reduced to half of that of pure **R1** (Fig. 2a), suggesting an alteration in the molar absorptivity coefficient of the **R1**– Hg^{2+} complex. On the other hand, **R2** and **R3** solutions were almost non-responsive upon treatment with Hg^{2+} (Fig. S1, ESI[†]).

The fluorescence study of **R1** showed an emission maximum at 485 nm, when excited at 410 nm. No excitation dependent emission wavelength shift was observed for **R1**. The fluorescence quantum yield (Φ_f) of **R1** was found to be 0.15 using Lucifer yellow CH ($\Phi_f = 0.27$ in water) as the reference. When the Hg^{2+} solution was added gradually up to 10.0 equivalents, fluorescence quenching was caused, thereby resulting in a 16 fold decrease in the quantum yield ($\Phi_f = 0.009$). The complexation of **R1** with Hg^{2+} , creating a drastic change in the fluorescence intensity, can be considered to be an on–off sensing response. This analysis suggested the better binding ability of **R1** to Hg^{2+} . The limit of detection (LOD) calculation^{47,48} using fluorescence titration data showed that

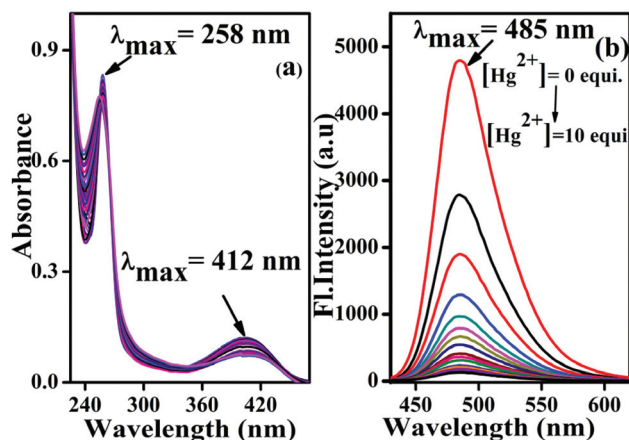


Fig. 2 (a) Absorption and (b) fluorescence titration spectra of **R1** with Hg^{2+} .

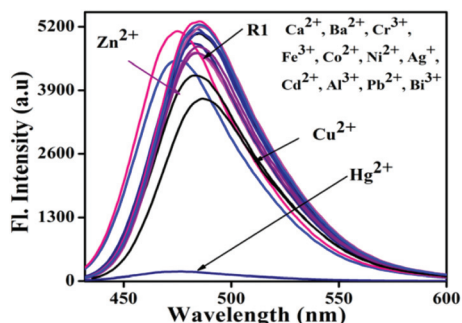


Fig. 3 Comparative fluorescence titration spectra of **R1** with Hg^{2+} and other metal ions in EtOH.

R1 could be used to sense very low-level concentration (1.72×10^{-7} M) of Hg^{2+} (Fig. S7, ESI[†]). A high binding efficiency of **R1** to Hg^{2+} ($K_a = 5.6 \times 10^4 \text{ M}^{-1}$) found from the Benesi–Hildebrand linear regression analysis^{49,50} also substantiated the significant affinity of **R1** towards Hg^{2+} (Fig. S6, ESI[†]).

The addition of other metal ions (except for Cu^{2+} and Zn^{2+}) up to 10.0 equivalents did not show any detectable change of quenching in the emission spectra of **R1**. However, the extent of quenching in the presence of both the ions was found to be much less than Hg^{2+} (Fig. 3). On the other side, emissions of **R2** and **R3** remained unresponsive upon the addition of either Hg^{2+} or other metal ions (Fig. S1, ESI[†]).

The reversibility of complexation between the sensor and the metal ion was carried out using EDTA as a chelating agent. Upon the addition of 1.0 equivalent of EDTA, the emission intensity gradually increased, leading to the formation of the EDTA- Hg^{2+} complex (Fig. S8, ESI[†]). However, the intensity decreased again upon the addition of excess Hg^{2+} , confirming the reversible complexation nature of the sensor with Hg^{2+} . To reproduce the reversible complexation of the receptor, the same experiment was performed using I^- , which showed a similar result (Fig. S9, ESI[†]). The pH-responsive emissions of **R1** and **R1-Hg**²⁺ complex were performed in order to have a comparison with the human physiological system. The respective intensities of the emission maxima (485 nm) were plotted against pH (Fig. 4). For **R1**, the correlation was found to be

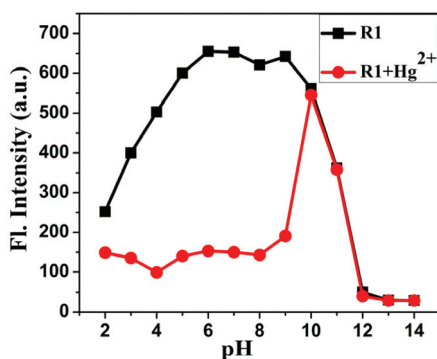


Fig. 4 Influence of pH of **R1** ($\lambda_{\text{em}} = 485 \text{ nm}$) and **R1-Hg**²⁺ complex ($\lambda_{\text{ex}} = 410 \text{ nm}$).

Gaussian in nature, with the maximum intensity being between pH 6 and 7. In contrast, for the **R1-Hg**²⁺ complex, the sharp peak in between pH 9 and 12, centered around pH 10, indicated that the stability of the **R1-Hg**²⁺ complex remained unaffected in the entire acidic region and well above neutral pH. Actually, for the whole pH range of 5–9, **R1-Hg**²⁺ remained quite stable and thus could be found to be compatible with the human physiological system.

Time-resolved fluorescence measurement

Upon gradual addition of Hg^{2+} to **R1**, the emission intensities at 420 nm remained unchanged, while a steady quenching was observed at 485 nm. Fluorescence decays were measured using a time-correlated single photon counting system from IBH, using 340 nm (λ_{max} of the quinoline absorption band) as the excitation wavelength. The FWHM of the excitation pulse was 1.23 ns, and a temporal resolution of 7.14 ps was used. Fluorescence decay traces were recorded at 485 nm which showed that upon addition of Hg^{2+} (**R1** : Hg^{2+} = 1 : 9), the single exponential decay of **R1** (Fig. 5) transformed into a bi-modal form with the faster component found to be of the order of 600 ps and the slower one 2.5 ns (similar to the **R1** lifetime at 485 nm). Upon gradual addition of Hg^{2+} , the faster component (600 ps) remained unchanged, but its contribution increased steadily (Table T2, ESI[†]), while the slower component (the emissive state) became even slightly slower with its contribution being decreased by ~10% (up to **R1** : Hg^{2+} = 1 : 1). It was suggested that upon gradual addition of Hg^{2+} , more **R1-Hg**²⁺ complex, involved in the non-radiative process, was formed and the increase in population was reflected by the rise in the contribution of the faster component, while the complex formation somewhat stabilized the emissive state (the lifetime of the emissive state was 3.3 ns). Similarly, steady-state and time-resolved studies were performed using Cu^{2+} , Cd^{2+} and Zn^{2+} . Upon the addition of Cu^{2+} , substantial quenching was observed in the steady-state emission of **R1**. However, the decay traces of pure **R1** were unaltered (Fig. S4, ESI[†]), indicat-

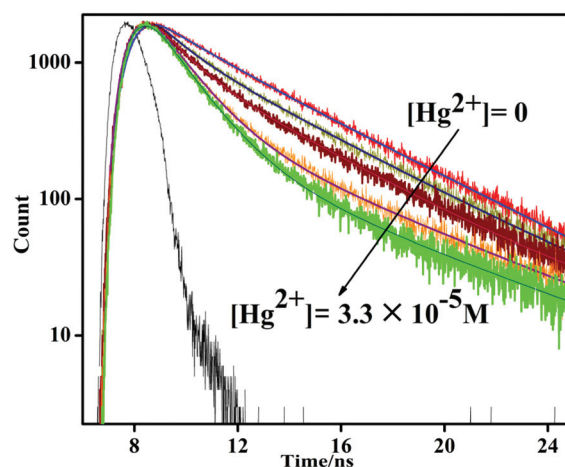


Fig. 5 Fluorescence decay traces of **R1** with and without Hg^{2+} ($\lambda_{\text{ex}} = 315 \text{ nm}$ and $\lambda_{\text{em}} = 485 \text{ nm}$).

ing that an ultrafast pathway may be associated with the quenching process. However, there was no change in the emission spectra of **R1** upon addition of Cd^{2+} , but decay traces were found to be faster in **R1** itself. This hints about the possible missing out of the predominant component, unresolvable by our time-resolved experimental setup. On the other hand, steady-state and time-resolved data of **R1**, in the presence of Zn^{2+} corroborated each other and demonstrated similar observations found in the case of Hg^{2+} .

It was also imperative to perform time-resolved fluorescence study of the sensor to establish if PET (photoinduced electron transfer) or FRET (fluorescence resonance energy transfer) was responsible for the excited state dynamics in order to understand the origin of the quenching process in the presence of Hg^{2+} . The sensor **R1** is composed of quinoline and coumarin moiety. As the emission of quinoline overlaps with the absorption band of coumarin (Fig. 6a), it is expected that energy transfer will take place *via* the dipole-dipole interaction from quinoline to coumarin. This has been proposed for a number of incidents, bearing similar moieties.⁴¹ However, it was essential to check if there is indeed an energy transfer from quinoline to coumarin. For an effective FRET process, upon addition of coumarin to the quinoline solution, the fluorescence intensity of the former should increase with a concomitant decrease in the fluorescence intensity of the latter. In a steady-state experiment upon constant addition of coumarin to quinoline, the fluorescence intensity of quinoline indeed decreased with an increase in coumarin emission (Fig. 6b). In time-resolved fluorescence, on the other hand, FRET would have been established if the fluorescence decays of quinoline become faster, while those of coumarin became slower when the latter was added to the former. However, no such characteristic peak was observed in this particular case. Quinoline decay at its emission maximum (420 nm) was bimodal, whereas coumarin (λ_{em}

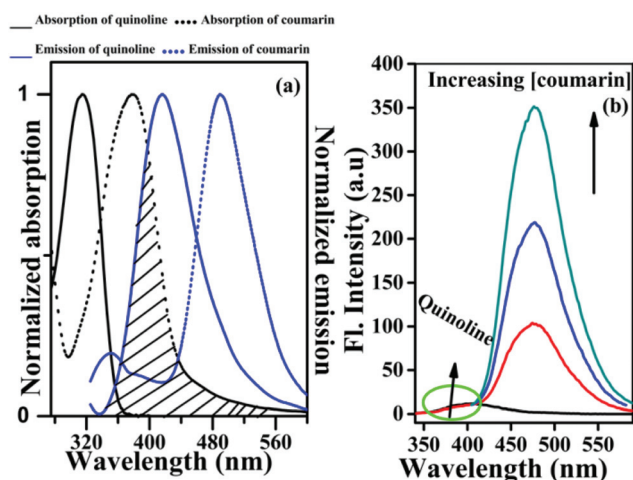


Fig. 6 (a) Normalized absorption and emission spectra of quinoline and coumarin amine in ethanol (black and blue straight lines for absorptions and dotted lines for emissions of quinoline and coumarin respectively). (b) Steady state emission spectra of quinoline with increasing concentration of coumarin.

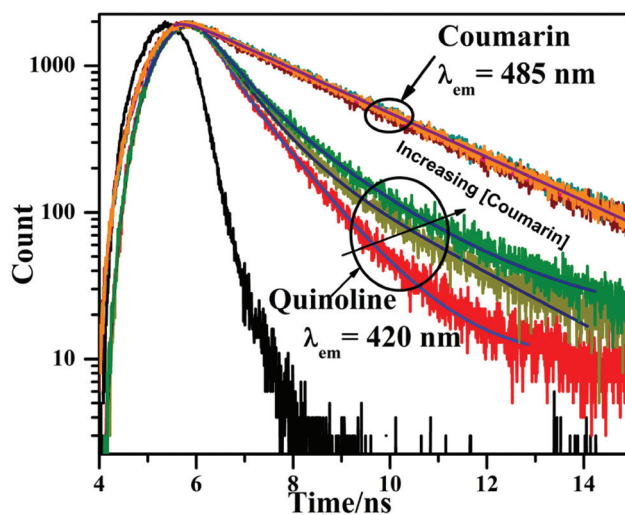


Fig. 7 Fluorescence decay traces of quinoline with varying concentrations of coumarin ($\lambda_{\text{ex}} = 340 \text{ nm}$).

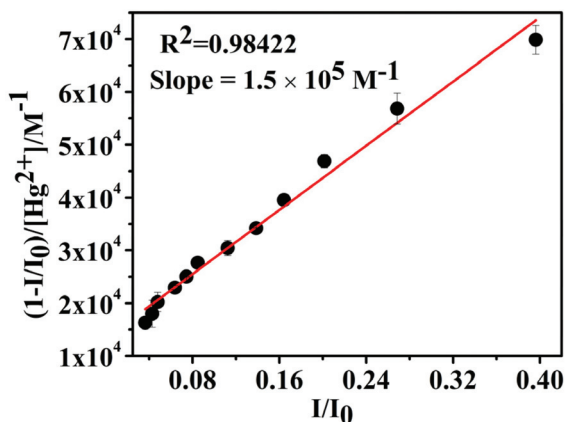
= 485 nm) decay was found to be single exponential in nature (Table T1, ESI†). On the addition of coumarin and monitoring at the quinoline emission maximum (420 nm), faster decays were not observed and while monitored at the coumarin emission maximum (485 nm), the decays remained unchanged (Fig. 7). To elaborate, upon gradual addition of coumarin, while keeping the quinoline concentration constant, and monitoring at quinoline emission, the longer component of the decay traces became slower and the shortest component was unaffected (Fig. 7). However, there was no change in the decay traces monitored at coumarin emission with varying concentrations of coumarin. This nullifies the possibility of FRET and suggests that if there is indeed any energy transfer through the dipole-dipole interaction, it is within an ultrafast time scale and thus cannot be resolved by our system. However, the computational calculation (explained later under ‘quantum chemical TDDFT calculation’ heading) reveals PET to be the origin of the non-radiative channel for this compound. The decay traces of **R1**, monitored at 420 nm and 485 nm respectively (*i.e.* at the quinoline and coumarin emission maximum respectively) were found to be following the characteristics of the quinoline-coumarin (2:1) mixture (at respective emission wavelengths), suggesting almost unaltered nature of quinoline and coumarin in **R1** (Fig. S5, ESI†). However, it was also found that in **R1**, the quinoline moiety got stabilized with respect to free quinoline, substantiated by a longer lifetime (Table T1, ESI†), indicating that triazole bridged quinoline experiences more rigidity.

Stern-Volmer plot

In order to find out the efficiency and the nature of the quenching process in the presence of Hg^{2+} , Stern-Volmer plots were obtained from the steady-state and time-resolved fluorescence studies. K_{SV}^0 , the steady-state rate constant, and the corresponding k_{q}^0 were calculated from the lower part of the S-V plot (Table 1, Fig. S3, ESI†) using eqn (1). However, it was

Table 1 The values of S–V constant and bimolecular quenching rate constant

Sr. no.	S–V constant K_{sv}^0 ($\times 10^5 \text{ M}^{-1}$)	Bimolecular quenching rate constant k_q ($\times 10^{14} \text{ mol}^{-1} \text{ L s}^{-1}$)
1	2.3	0.958
2	1.5	0.625

**Fig. 8** Modified S–V plot.

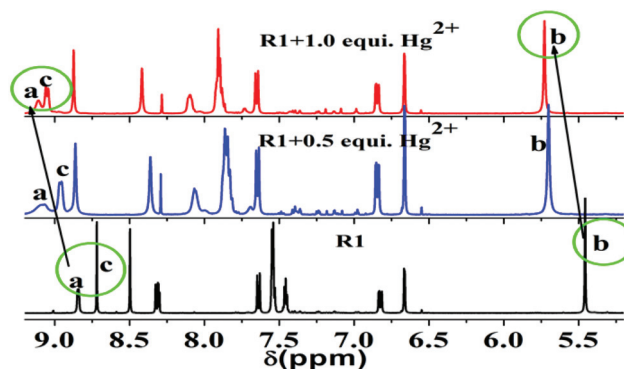
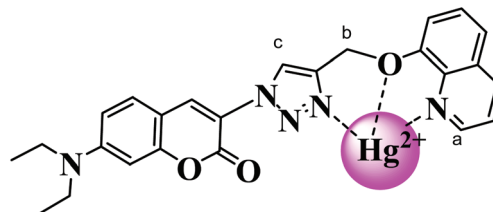
found that at higher concentration of Hg^{2+} , S–V plot deviated from linearity (the inset plot of Fig. S3, ESI†), indicating the onset of static quenching. Therefore, the dynamic quenching constant (K_{sv}) and the bimolecular quenching rate constant (k_q , as $K_{sv} = k_q\tau_0$) parameters were obtained using the linear part of the modified S–V equation (eqn (2)) following the ‘sphere of action static quenching model’⁵¹ (Fig. 8). The dynamic quenching constant and bimolecular quenching rate constants are given in Table 1.

$$\frac{I_0}{I} = 1 + K_{sv}[Q] \quad (1)$$

$$\frac{1 - \frac{I}{I_0}}{[Q]} = K_{sv} \left(\frac{I}{I_0} \right) + \frac{(1 - w)}{[Q]} \quad (2)$$

NMR study

The ^1H NMR study of **R1** with Hg^{2+} at room temperature (298 K) has been performed to have an insight into complexation. Fig. 9 represents the distinguished chemical shift of the proton adjacent to quinoline N (H_a), methylene proton (H_b), and triazole ring hydrogen (H_c) at δ 8.85, 5.46, and 8.72 ppm respectively (as mentioned in Fig. 10). Upon addition of 0.5 equivalent of Hg^{2+} , the aforementioned peaks shifted to δ 8.97, 5.70, and 8.86 ppm, respectively. Upon addition of 1.0 equivalent of Hg^{2+} , the peaks again showed a downfield shift from the previous observation, and the respective values were δ 9.04, 5.73, and 8.87 ppm. Therefore, it can be revealed that both the quinoline and triazole moieties actively take part in the complexation. The signal broadening occurred after a certain point

**Fig. 9** ^1H -NMR spectra of **R1** with varying amounts of Hg^{2+} in d_6 -DMSO.**Fig. 10** Probable binding mode of complexation of **R1** with Hg^{2+} .

due to the paramagnetic effect which overwhelmed the spectrum with increasing the concentration of Hg^{2+} .⁵²

Possible binding mode

The possible binding mode of **R1** is depicted in Fig. 10, where the suitable cavity for Hg^{2+} encapsulation was formed by the electronegative ‘O’ atom, ring ‘N’ atom of quinoline and one ‘N-3’ atom of triazole. On the other hand, no cavity for Hg^{2+} was formed by **R2** and **R3** due to the absence of quinoline ‘N’. DFT calculations and the NMR study also supported the probable binding mode of **R1**. The FT-IR spectra of **R1** and **R1–Hg²⁺** were obtained (ESI†). Upon addition of Hg^{2+} to **R1**, the C–H band of triazole was shifted from 3133 cm^{-1} to 3120 cm^{-1} and the C–O band of quinoline was shifted sharply from 1129 cm^{-1} to 1060 cm^{-1} indicating the participation of triazole and the ether subunit in **R1–Hg²⁺** complexation. In addition to that, a new band was found at 610 cm^{-1} , which again suggested the participation of quinoline ‘N’ in complexation. The MS value of the sensor **R1** was detected at m/z 441.1801, whereas the value of m/z 678.1401 was regarded as $[\text{R1} + \text{Hg} + 2\text{H}_2\text{O} - \text{H}]$.

Quantum chemical (TDDFT) calculations

Quantum chemical calculations were performed to understand the nature of metal binding with **R1**. The geometrical optimizations of **R1** and its complex were carried out using the B3LYP functional, and the 6-311g** basis set was used for C, H, N, and O atoms, whereas LANL2DZ effective core potential (ECP) was used for Hg^{2+} , as implemented using the TeraChem Software.^{53–55} All calculations were performed in the gas

phase. The initial coordinates for the geometry optimization were obtained from *ab initio* molecular dynamics (AIMD) simulations. AIMD simulations were performed using the 3-21g basis set at the HF level and the temperature was set to 300 K. The binding energy (E_B) between the Hg^{2+} and **R1** was calculated using the following equation:

$$E_B = E_{\text{comp}} - E_{\text{R1}} - E_{\text{Hg}^{2+}}$$

where, E_{comp} , E_{R1} , and $E_{\text{Hg}^{2+}}$ are the ground state optimized energies of the **R1**– Hg^{2+} complex, **R1**, and Hg^{2+} , respectively. Two binding modes have been observed during the geometry optimizations, as shown in Fig. 11. The binding mode **A** was found to be more stable than the binding mode **B** by 20.867 kcal mol^{−1} (see Table T3, ESI†).

In order to reveal the intricate details of the electronic structure of both the binding modes, the excited state highest occupied molecular orbital (HOMO) and the lowest unoccupied molecular orbital (LUMO) for the **R1** and **R1**– Hg^{2+} complexes (mode A and mode B) under vacuum were calculated from their optimized structures by the TDDFT method using the 6-311g** basis set, as shown in Fig. 12. In the case of **R1**, the HOMO was spread mainly over coumarin and triazole, whereas the LUMO is partially on the coumarin and triazole ring. After the complexation with Hg^{2+} (**binding mode A**), the HOMO now resided on the Hg^{2+} ion and partially on quinoline and triazole nitrogen atoms, whereas the LUMO was over the coumarin ring. The energy difference between the HOMO and the LUMO of **R1** and **R1**– Hg^{2+} (**binding mode A**) were 83.207 kcal mol^{−1} and 14.495 kcal mol^{−1}, respectively. These results showed that the binding of Hg^{2+} with **R1** (**mode A**) lowered the energy gap between the HOMO and the LUMO of the complex and stabilized the system. The energy gap of the **R1**– Hg^{2+} complex on the **A**-mode (14.495 kcal mol^{−1}) is higher than that on the **B**-mode (7.216 kcal mol^{−1}), revealing that the excitation of Hg^{2+} ion attached to **R1** on the **B**-mode occurred more easily than that on the **A**-mode. This indicates that the **R1**– Hg^{2+} complex on the **A**-mode has higher stability than on

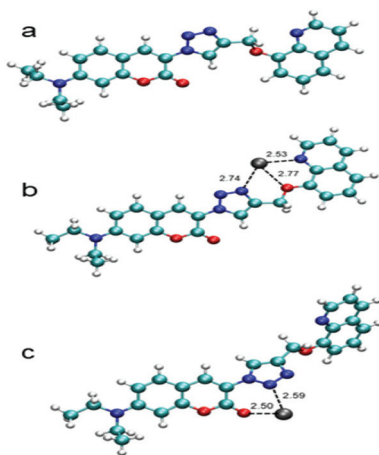


Fig. 11 Optimized structures of (a) sensor, **R1**; (b) **R1**– Hg^{2+} complex on **A** mode; (c) **R1**– Hg^{2+} complex on **B** mode.

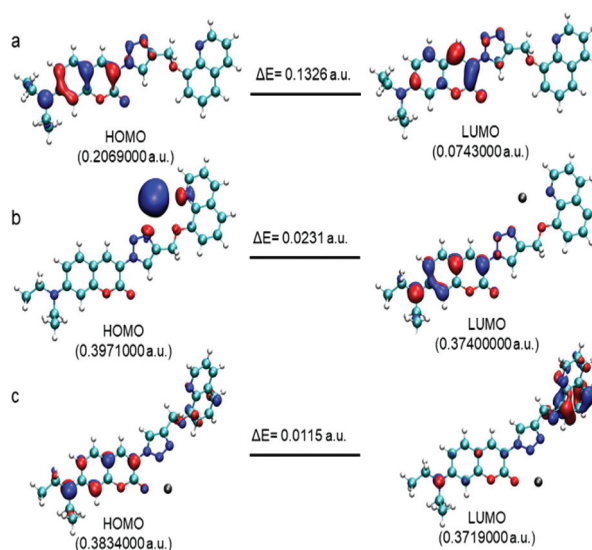


Fig. 12 Excited-state HOMO–LUMO diagrams; (a) free sensor, **R1**; (b) **R1**– Hg^{2+} complex on **A** binding mode; (c) **R1**– Hg^{2+} complex on **B** binding mode.

the **B**-mode at the ground state which is also realized by the binding energy difference between the two modes (Table T3, ESI†). The HOMO to LUMO excitation of **R1** was found to be charge transfer with the largest CI coefficient of -0.686911 .

To confirm the exact mechanism of fluorescence quenching upon addition of Hg^{2+} , the TDDFT study was carried out. Generally, the PET-based fluorescent probes contained three units as fluorophore and chelator, which was separated by the third unit *i.e.*, a short aliphatic spacer. As shown in Fig. S12 (ESI†), the LUMO of the electron-poor chelator (quinoline moiety) lies just below the LUMO of the excited fluorophore (coumarin moiety) so that the singly excited LUMO of the coumarin moiety donated an electron to the LUMO of quinoline, an example of typical d-PET mechanism.⁵⁶ Upon complexation of **R1** with Hg^{2+} , the chelator became more electron-poor and the corresponding energy of the LUMO of the chelator was further reduced, and thus the PET was accelerated, leading to fluorescence quenching.

Biological application

Cell culture. U-2 OS (ATCC® HTB-96™) cells were grown in RPMI-1640 supplemented with 10% FBS at 37 °C under 5% CO₂. Cells were placed in a 48 or 96 well culture plate and allowed to adhere for 48 hours before experimentation.

Cell viability assay. First, stock solutions of **R1** and **R2** were prepared in H₂O/ethanol solution (1 : 1, v/v) in such a way that during experimentation, it was further diluted in water to maintain the ratio of 1 : 5 (stock : water). This minimized the cellular toxicity caused by ethanol.

The methyl thiazolyl tetrazolium (MTT) assay has been used to measure the cytotoxic potential of **R1** and **R2** in U-2 OS cells. These cells were seeded in a 96-well cell-culture plate. Various concentrations (5, 10, 25 and 50 μM) of **R1** and **R2**

were added to the cells. Then, these were incubated at 37 °C under 5% CO₂ for 24 hours. The MTT solution (10 μL, 5 mg mL⁻¹) was added to each well and incubated at 37 °C under 5% CO₂ for 4 hours. The MTT solution was removed and the yellow precipitates (formazan) observed in plates were dissolved in 200 μL of acidic isopropanol. A Multiskan™ GO Microplate Spectrophotometer was used to measure the absorbance at 570 nm for each well. The viability of cells was calculated according to the following equation:

$$\% \text{Cell viability} = [\text{experimental OD}_{570} / \text{control OD}_{570}] \times 100$$

Fluorescence imaging in cells

U-2 OS cells were placed in a 48 well cell-culture plate and allowed to adhere for 48 hours. To assess the Hg²⁺ sensing capacity of **R1** and **R2**, initially uptakes of **R1** and **R2** were prepared in phosphate-buffered saline (PBS). Then the cells were treated with 35 μM of **R1** and **R2** respectively and incubated for 2 h. After the culture medium was removed, the treated cells were washed with PBS before observation. Fluorescence images of the cells were obtained using the EVOS® FL Cell Imaging System. Then Hg(ClO₄)₂, dissolved in sterile PBS (pH = 7.4), was added at 1.5 μM concentration to the desired experimental wells and incubated at 37 °C for another 30 minutes. The treated cells were again washed with PBS to wash out the remaining metal ions. Again, the fluorescence images of the cells were obtained in an interval of 30 min and 60 min using the EVOS® FL Cell Imaging System (Life Technologies, USA). The potential of 8-hydroxy quinoline appended coumarin-triazole chemosensor (**R1**) for sensing Hg²⁺ in living cells was also examined. The MTT assay for U-2 OS (osteosarcoma cell line) cells was used to determine the cyto-compatibility of **R1**. The cell viability was found to be more than 80% (Fig. 13) following treatment with the compound for 24 hours. This result indicated that **R1** was safe and induced low cytotoxicity even at higher concentration (50 μM).

Imaging analyses were performed for demonstrating the bio-distribution of the compound **R1** and sensing Hg²⁺ in living cells using the EVOS® FL Cell Imaging System. U-2 OS cells that were incubated with Hg²⁺ only did not produce any

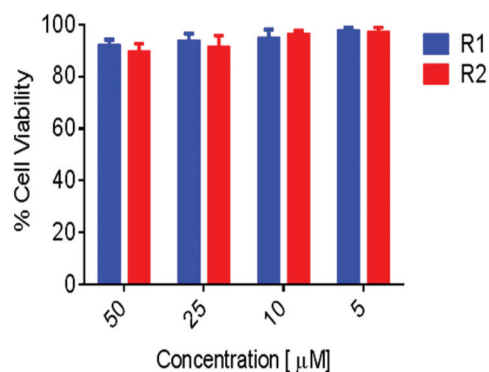


Fig. 13 MTT assay of U-2-OS cells treated in the presence of **R1** and **R2** (0–50 μM) incubated at 37 °C for 24 hours.

detectable fluorescence (Fig. 14d–f). However, upon treatment with **R1** or **R2**, a bright green fluorescence was observed in the U-2OS cells (Fig. 14a–c & 15a–e). Overlaying of fluorescence

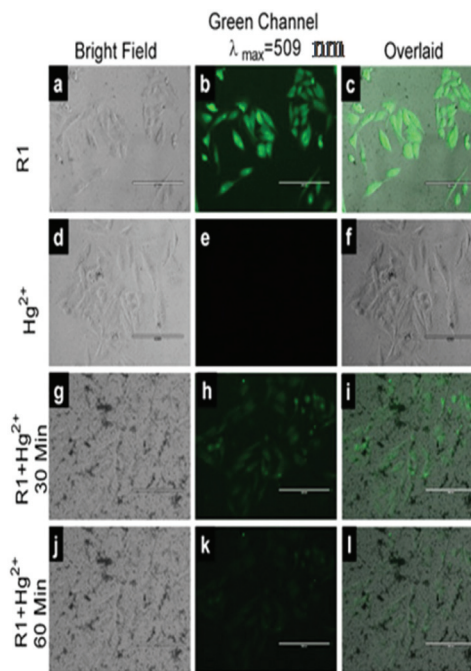


Fig. 14 Fluorescence images of U-2-OS cells treated with **R1** (a–c) and Hg²⁺ after 0 min (d–f), 30 min (g–i) & 60 min (j–l). (Left) Bright field images; (middle) fluorescence images in green channel and (right) overlaid images. Magnification 400x.

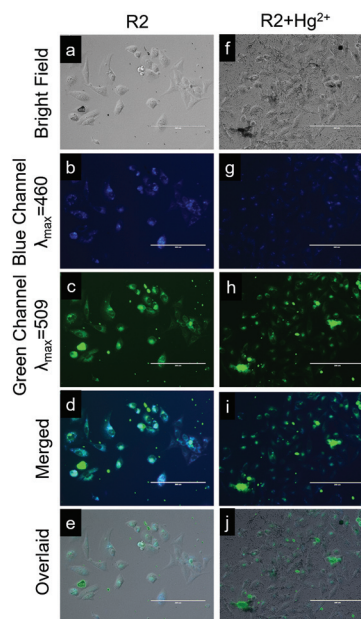


Fig. 15 Fluorescence images of U-2-OS cells treated with **R2** (1–e) and **R2**+Hg²⁺ (f–j). (a–f) bright field images, images taken in blue (b–g) and green (c–h) channel, images of U2OS cells after merging all the channels (d–i) and after overlay with a bright field (e–j). Magnification 400x.

and bright-field images confirmed that the fluorescence signals were localized in the intracellular areas, which indicated efficient cell-membrane permeability for **R1** and **R2**. The specificity of **R1** towards **Hg2+** was demonstrated by performing similar experiments using **Hg2+**. Upon the addition of **Hg2+** treated with **R1** and **R2**, the fluorescence images were obtained at intervals of 30 min and 60 min. Due to the presence of **Hg2+**, the bright green fluorescence intensity of **R1** was reduced in a time-dependent manner (Fig. 14g–i). After 60 minutes of addition, there was almost no or very low level of fluorescence (Fig. 14j–i). But in the case of **R2** the attenuation of fluorescence intensity in U-2-OS cells was found to be negligibly lower than that in the case of **R1** (Fig. 15f–j). In contrast to **R1**, **R2** displayed blue fluorescence rather than green colour at a concentration of 35 μM being tested (Fig. 14b and 15g). These observations demonstrated that **R1** was much more selective than **R2** to detect **Hg2+** in living cells.

Conclusions

A hydroxyquinoline appended coumarin–triazole conjugated chemosensor (**R1**) has been developed for selective sensing of **Hg2+**, which exhibits a turn-off response. The study of the excited state processes of this compound revealed an unusual PET (photoinduced energy transfer), and not FRET (Förster resonance energy transfer), unlike similar types of compounds, to be the key associated photophysical process. This chemosensor can potentially be applied for the fluorescence imaging of living cells. Moreover, it exhibits low cytotoxicity and, therefore, can be used for *in vivo* detection of **Hg2+**. The 'N' atom of quinoline (**R1**) has been found to play a crucial role in forming a suitable cavity for **Hg2+** detection, as evidenced by the absence of the 'N' atom of quinoline (quinoline was replaced by benzene and naphthalene respectively) in **R2** and **R3**, for which any detectable change in the presence of **Hg2+** was not observed.

Experimental

General

All reagents (AR grade) for synthesis were purchased from Sigma-Aldrich chemicals and used without further purification. All metal perchlorate salts were prepared from the corresponding metal carbonates. Solvents were dried following standard procedures. UV-grade ethanol was used for UV-Vis and fluorescence titration. ^1H NMR spectra were recorded on a Bruker AV400 instrument using CDCl_3 and $\text{d}_6\text{-DMSO}$ solvents with TMS as the internal standard. ESI-MS measurements were carried out using a microTOF-Q II 10337 mass spectrometer instrument. FTIR spectra were measured using a Spectrum 2000 Perkin-Elmer Spectrometer. UV-Vis spectra and fluorescence spectra were recorded using a UV-Lambda 365 PerkinElmer Spectrophotometer (1.0 cm quartz cell) and a Perkin-Elmer LS 55 Fluorescence spectrometer, respectively. Single-crystal XRD data were collected using a SuperNova

G8910B. Melting points were determined using a Remco hot-coil stage melting point apparatus.

Preparation of 3-azido-7-(diethylamino)-2H-chromen-2-one (compound 1)

Initially, 7-diethylamino-3-amino coumarin was prepared according to the reported procedure⁴⁶ (see details in the Experimental section, ESI†), and then it (100 mg, 0.43 mmol) was dissolved slowly in aq. HCl (17.2%, 4.0 mL) at room temperature. After being cooled at 0 $^\circ\text{C}$ –5 $^\circ\text{C}$ and consequent addition of NaNO_2 solution (30 mg, 0.43 mmol), the reaction mixture was continuously stirred for 1.0 hour at 0–5 $^\circ\text{C}$. This was followed by the addition of potassium acetate (2.0 g) in water (5.0 mL) to adjust the pH of the resulting solution to 4.0. Sodium azide (57 mg, 0.88 mmol) was added in portions at 0–5 $^\circ\text{C}$, and the mixture was stirred for another five hours maintaining the same temperature. Then, the precipitated product was rapidly filtered, washed with ice-cold water (10.0 mL) and dried under vacuum to yield the final product as a yellow solid (yield: 84%).

General procedure for the preparation of compound 2, 3, and 4

For the preparation of compound 2, 3, and 4, to the solutions of 8-hydroxy quinoline, benzyl alcohol, and 1-naphthol respectively (1.0 equiv.) in acetone (20 mL), anhydrous potassium carbonate (1.5 equiv.) was added and the solution was stirred at room temperature under an argon atmosphere. Propargyl bromide (1.5 equiv.) was added to the solution and the resulting mixture was refluxed for 5 h. After completion of the reaction, the solvent was dried, and the crude solid was partitioned between ethyl acetate and water. The ethyl acetate layer was collected and the process was repeated three times. The combined organic extract was dried over anhydrous Na_2SO_4 , concentrated under vacuum and purified by column chromatography.

8-(Prop-2-ynyloxy) quinoline (compound 2). ^1H NMR (400 MHz, CDCl_3): δ 8.60 (s, 1H), 7.76 (d, J = 4.0 Hz, 1H), 7.10 (m, J = 8.0 Hz, 3H), 6.92 (d, J = 8.0 Hz, 1H), 4.70 (s, 2H), 2.24 (s, 1H); ^{13}C NMR (CDCl_3 , 100 MHz) δ 149.36, 135.86, 126.37, 121.65, 120.59, 109.86, 78.26, 76.12, 56.41; FTIR (KBr, cm^{-1}): 3303, 1502, 1490, (yield 85%).

1-(Prop2-ynyloxy) benzene (compound 3). ^1H NMR (400 MHz, CDCl_3): δ 7.161 (t, J = 8.4 Hz, 3H), 6.85 (q, J = 8.0 Hz, 3H), 4.51 (s, 2H), 2.37 (s, 1H); ^{13}C NMR (CDCl_3 , 100 MHz) δ 157.63, 129.59, 121.66, 114.98, 78.78, 75.66, 55.75; FTIR (KBr, cm^{-1}): 3296, 1599, 1494, (yield 80%).

1-(Prop2-ynyloxy) naphthalene (compound 4). ^1H NMR (400 MHz, CDCl_3): δ 8.37 (s, 1H), 7.89 (s, 1H), 7.56 (m, 3H), 7.45 (t, J = 7.6 Hz, 1H), 7.00 (s, 1H), 4.94 (s, 1H), 2.62 (t, J = 2.4 Hz, 1H); ^{13}C NMR (CDCl_3 , 100 MHz): δ 155.2, 134.4, 127.4, 126.4, 125.4, 125.3, 121.9, 121.13, 105.4, 78.5, 75.5, 56.0, (yield 90%).

General procedure for the preparation of compound R1, R2 and R3

For the preparation of **R1**, **R2** and **R3**, compound 2, 3 and 4 (1 equiv.) were dissolved separately in 80 ml of the 1 : 1 DCM/

EtOH mixture. Then compound **1** (1 equiv.), sodium ascorbate (1.5 equiv.) and copper sulfate (1.5 equiv.) were added to this solution. The resulting mixture was stirred for 24 h at room temperature. Upon completion of the reaction, the mixture was filtered, extracted with ethyl acetate, concentrated under vacuum and then subjected to column chromatography to obtain the desired product.

7-Diethylamino-3-(4-((quinoline-8-yloxy)methyl)-1H-1,2,3-triazol-yl)-2H-chromen-2-one (R1). $^1\text{H NMR}$ of **R1** (400 MHz, CDCl_3): δ 8.95 (s, 1H), 8.78 (s, 1H), 8.34 (s, J 1H), 8.12 (d, 8.0 Hz, 1H), 7.43–7.38 (m, 5H), 6.66 (d, 8.0 Hz, 1H), 6.62 (s, 1H), 5.62 (s, 2H), 3.44 (q, J = 8.0 Hz, 4H), 1.23 (t, J = 8.0 Hz, 6H); $^{13}\text{C NMR}$ (CDCl_3 , 125 MHz): δ 156.5, 155.4, 153.5, 151.2, 149.0, 143.2, 139.9, 135.6, 134.6, 129.6, 129.1, 126.3, 126.2, 124.2, 121.3, 120.1, 119.9, 109.5, 96.6, 44.6, 29.2, 12.0; **HRMS (ESI) (R1)**: calculated for $\text{C}_{25}\text{H}_{23}\text{N}_5\text{O}_3$ m/z 442.1873 $[\text{M} + \text{H}]^+$, **found**: 442.1874; **FT-IR (KBr, cm^{-1})**: 3131 (triazole C–H), 1730 (C=O str.), 1609 (C=N str.), 1400 (C–N str.), m.p 155–157 °C, (163.8 mg, yield 68%).

7-Diethylamino-3-(4-((phenoxy)methyl)-1H-1,2,3-triazol-yl)-2H-chromen-2-one (R2). $^1\text{H NMR}$ (500 MHz, CDCl_3): δ 8.64 (s, 1H), 8.39 (s, 1H), 7.41 (d, 1H, J = 14.5 Hz), 7.30 (2H, d, J = 7.5 Hz), 7.03 (2H, d, J = 8.5 Hz), 6.97 (t, J = 6.5 Hz, 1H), 6.68 (d, J = 9.0 Hz, 1H), 6.56 (s, 1H), 5.27 (s, 2H), 3.46 (q, J = 7.0 Hz, 4H), 1.24 (t, J = 7.0 Hz, 6H); $^{13}\text{C NMR}$ (100 MHz, CDCl_3): 168.0, 166.2, 158.2, 158.1, 144.7, 144.4, 129.8, 124.5, 124.3, 121.4, 121.3, 114.8, 62.5, 51.0, 14.0; **HRMS (ESI) (R2)**: calculated for $\text{C}_{22}\text{H}_{22}\text{N}_4\text{O}_3$ m/z 391.1764 $[\text{M} + \text{H}]^+$, **found**: 391.4071; **FT-IR (KBr, cm^{-1})**: 3130, 1712, 1609, 1400, m.p 129–131 °C, (206.8 mg, yield 70%).

7-Diethylamino-3-(4-((naphthalene-1-yloxy)-1H-1,2,3-triazol-yl)-2H-chromen-2-one (R3). $^1\text{H NMR}$ (400 MHz, CDCl_3): δ 8.71 (s, 1H), 8.41 (s, 1H), 8.29 (d, 1H, J = 6.8 Hz), 7.48 (s, 1H), 7.43–7.39 (5H, m), 7.03 (d, J = 6.8 Hz, 1H), 6.68 (d, J = 7.5 Hz, 1H), 6.56 (s, 1H), 5.46 (s, 2H), 3.46 (q, J = 6.8 Hz, 4H), 1.24 (t, J = 5.6 Hz, 6H); $^{13}\text{C NMR}$ (100 MHz, CDCl_3): 157.0, 155.9, 154.1, 151.7, 130.1, 127.4, 126.5, 125.8, 125.3, 123.9, 122.2, 116.8, 110.2, 107.0, 105.3, 97.0, 62.2, 45.0, 12.4; **HRMS (ESI) (R3)**: calculated for $\text{C}_{26}\text{H}_{24}\text{N}_4\text{O}_3$ m/z 441.1921 $[\text{M} + \text{H}]^+$, **found**: 441.1915; **FT-IR (cm^{-1})**: 3134, 1712, 1609, 1400. m.p 147–149 °C, (169.2 mg, yield 70%).

Conflicts of interest

There are no conflicts to declare.

Acknowledgements

SD acknowledges SERB-DST (project no. EMR/2016/002183), Govt. of India for the financial assistance and DST-FIST (project no. SR/FST/CSI-256) for providing a grant to install 400 MHz NMR facility in the Department of Chemistry, IIT (ISM), Dhanbad. Authors are thankful to Prof. Samita Basu and Dr Padmaja P Mishra, Saha Institute of Nuclear Physics, Kolkata, India, for providing TCSPC facility.

Notes and references

- 1 R. K. Mahajan, R. Kaur, V. Bhalla, M. Kumar, T. Hattori and S. Miyano, Mercury(II) sensors based on calix [4] arene derivatives as receptor molecules, *Sens. Actuators, B*, 2008, **130**, 290–294.
- 2 A. Renzoni, F. Zino and E. Franchi, Mercury levels along the food chain and risk for exposed populations, *Environ. Res.*, 1998, **77**, 68–72.
- 3 D. Wu, W. Huang, Z. Lin, C. Duan, C. He, S. Wu and D. Wang, Highly sensitive multiresponsive chemosensor for selective detection of Hg^{2+} in natural water and different monitoring environments, *Inorg. Chem.*, 2008, **47**, 7190–7201.
- 4 X. Chen, K.-H. Baek, Y. Kim, S.-J. Kim, I. Shin and J. Yoon, A selenolactone-based fluorescent chemodosimeter to monitor mercury/methylmercury species in vitro and in vivo, *Tetrahedron*, 2010, **66**, 4016–4021.
- 5 T. Anand, G. Sivaraman and D. Chellappa, Hg^{2+} mediated quinazoline ensemble for highly selective recognition of Cysteine, *Spectrochim. Acta, Part A*, 2014, **123**, 18–24.
- 6 E. G. Pacyna, J. M. Pacyna, F. Steenhuisen and S. Wilson, Global anthropogenic mercury emission inventory for 2000, *Atmos. Environ.*, 2006, **40**, 4048–4063.
- 7 T. W. Clarkson and L. Magos, The toxicology of mercury and its chemical compounds, *Crit. Rev. Toxicol.*, 2006, **36**, 609–662.
- 8 K. A. Anderson, Mercury analysis in environmental samples by cold vapor techniques, in *Encyclopedia of Analytical Chemistry: Applications, Theory and Instrumentation*, 2006.
- 9 J. Lo, J. Yu, F. Hutchison and C. Wai, Solvent extraction of dithiocarbamate complexes and back-extraction with mercury(II) for determination of trace metals in seawater by atomic absorption spectrometry, *Anal. Chem.*, 1982, **54**, 2536–2539.
- 10 A. Panja and K. Ghosh, Selective sensing of Hg^{2+} via sol-gel transformation of a cholesterol-based compound, *Supramol. Chem.*, 2018, **30**, 722–729.
- 11 A. Panja and K. Ghosh, 4-Hydroxybenzaldehyde derived Schiff base gelators: case of the sustainability or rupturing of imine bonds towards the selective sensing of Ag^+ and Hg^{2+} ions via sol-gel methodology, *New J. Chem.*, 2019, **43**, 5139–5149.
- 12 S. Mondal, R. Raza and K. Ghosh, Cholesterol linked benzothiazole: A versatile gelator for detection of picric acid and metal ions such as Ag^+ , Hg^{2+} , Fe^{3+} and Al^{3+} under different conditions, *New J. Chem.*, 2019, **43**, 10509–10516.
- 13 A. Hemamalini and T. M. Das, Design and synthesis of sugar-triazole low molecular weight gels as mercury ion sensor, *New J. Chem.*, 2013, **37**, 2419–2425.
- 14 G. Aragay, J. Pons and A. Merkoçi, Recent trends in macro-, micro-, and nanomaterial-based tools and strategies for heavy-metal detection, *Chem. Rev.*, 2011, **111**, 3433–3458.
- 15 K. Kaur, R. Saini, A. Kumar, V. Luxami, N. Kaur, P. Singh and S. Kumar, Chemodosimeters: an approach for detec-

- tion and estimation of biologically and medically relevant metal ions, anions and thiols, *Coord. Chem. Rev.*, 2012, **256**, 1992–2028.
- 16 H. N. Kim, W. X. Ren, J. S. Kim and J. Yoon, Fluorescent and colorimetric sensors for detection of lead, cadmium, and mercury ions, *Chem. Soc. Rev.*, 2012, **41**, 3210–3244.
 - 17 D. Ray and P. Bharadwaj, A coumarin-derived fluorescence probe selective for magnesium, *Inorg. Chem.*, 2008, **47**, 2252–2254.
 - 18 N. C. Lim, J. V. Schuster, M. C. Porto, M. A. Tanudra, L. Yao, H. C. Freake and C. Brückner, Coumarin-based chemosensors for zinc(II): toward the determination of the design algorithm for CHEF-type and ratiometric probes, *Inorg. Chem.*, 2005, **44**, 2018–2030.
 - 19 M. Suresh and A. Das, New coumarin-based sensor molecule for magnesium and calcium ions, *Tetrahedron Lett.*, 2009, **50**, 5808–5812.
 - 20 H. S. Jung, J. H. Han, Z. H. Kim, C. Kang and J. S. Kim, Coumarin-Cu(II) ensemble-based cyanide sensing chemodosimeter, *Org. Lett.*, 2011, **13**, 5056–5059.
 - 21 K. Tsukamoto, Y. Shinohara, S. Iwasaki and H. Maeda, A coumarin-based fluorescent probe for Hg²⁺ and Ag⁺ with an N'-acetylthioureido group as a fluorescence switch, *Chem. Commun.*, 2011, **47**, 5073–5075.
 - 22 J. H. Kim, H. J. Kim, S. H. Kim, J. H. Lee, J. H. Do, H.-J. Kim, J. H. Lee and J. S. Kim, Fluorescent coumarinyl-dithiane as a selective chemodosimeter for mercury(II) ion in aqueous solution, *Tetrahedron Lett.*, 2009, **50**, 5958–5961.
 - 23 J. Wang, X. Qian and J. Cui, Detecting Hg²⁺ ions with an ICT fluorescent sensor molecule: remarkable emission spectra shift and unique selectivity, *J. Org. Chem.*, 2006, **71**, 4308–4311.
 - 24 J.-S. Wu, W.-M. Liu, X.-Q. Zhuang, F. Wang, P.-F. Wang, S.-L. Tao, X.-H. Zhang, S.-K. Wu and S.-T. Lee, Fluorescence turn on of coumarin derivatives by metal cations: a new signaling mechanism based on C=N isomerization, *Org. Lett.*, 2007, **9**, 33–36.
 - 25 H. S. Jung, P. S. Kwon, J. W. Lee, J. I. Kim, C. S. Hong, J. W. Kim, S. Yan, J. Y. Lee, J. H. Lee and T. Joo, Coumarin-derived Cu²⁺-selective fluorescence sensor: synthesis, mechanisms, and applications in living cells, *J. Am. Chem. Soc.*, 2009, **131**, 2008–2012.
 - 26 Y. Mei, P. A. Bentley and W. Wang, A selective and sensitive chemosensor for Cu²⁺ based on 8-hydroxyquinoline, *Tetrahedron Lett.*, 2006, **47**, 2447–2449.
 - 27 M. Mameli, M. C. Aragoni, M. Arca, C. Caltagirone, F. Demartin, G. Farruggia, G. De Filippo, F. A. Devillanova, A. Garau and F. Isaia, A Selective, Nontoxic, OFF-ON Fluorescent Molecular Sensor Based on 8-Hydroxyquinoline for Probing Cd²⁺ in Living Cells, *Chem. – Eur. J.*, 2010, **16**, 919–930.
 - 28 G. Farruggia, S. Iotti, L. Prodi, M. Montalti, N. Zaccheroni, P. B. Savage, V. Trapani, P. Sale and F. I. Wolf, 8-Hydroxyquinoline derivatives as fluorescent sensors for magnesium in living cells, *J. Am. Chem. Soc.*, 2006, **128**, 344–350.
 - 29 V. S. Mummdivarapu, K. Tabbasum, J. P. Chinta and C. P. Rao, 1, 3-Di-amidoquinoline conjugate of calix [4] arene (L) as a ratiometric and colorimetric sensor for Zn²⁺: Spectroscopy, microscopy and computational studies, *Dalton Trans.*, 2012, **41**, 1671–1674.
 - 30 Y. Mei and P. A. Bentley, A ratiometric fluorescent sensor for Zn²⁺ based on internal charge transfer (ICT), *Bioorg. Med. Chem. Lett.*, 2006, **16**, 3131–3134.
 - 31 Y. Zhao, Z. Lin, H. Liao, C. Duan and Q. Meng, A highly selective fluorescent chemosensor for Al³⁺ derived from 8-hydroxyquinoline, *Inorg. Chem. Commun.*, 2006, **9**, 966–968.
 - 32 K. C. Song, J. S. Kim, S. M. Park, K.-C. Chung, S. Ahn and S.-K. Chang, Fluorogenic Hg²⁺-selective chemodosimeter derived from 8-hydroxyquinoline, *Org. Lett.*, 2006, **8**, 3413–3416.
 - 33 I.-T. Ho, T.-L. Lai, R.-T. Wu, M.-T. Tsai, C.-M. Wu, G.-H. Lee and W.-S. Chung, Design and synthesis of triazolyl coumarins as Hg²⁺ selective fluorescent chemosensors, *Analyst*, 2012, **137**, 5770–5776.
 - 34 Q. Zhu, L. Li, L. Mu, X. Zeng, C. Redshaw and G. Wei, A ratiometric Al³⁺ ion probe based on the coumarin-quinoline FRET system, *J. Photochem. Photobiol.*, 2016, **328**, 217–224.
 - 35 D. Maity and T. Govindaraju, A differentially selective sensor with fluorescence turn-on response to Zn²⁺ and dual-mode ratiometric response to Al³⁺ in aqueous media, *Chem. Commun.*, 2012, **48**, 1039–1041.
 - 36 C. Kumari, D. Sain, A. Kumar, S. Debnath, P. Saha and S. Dey, Intracellular detection of hazardous Cd²⁺ through a fluorescence imaging technique by using a nontoxic coumarin based sensor, *Dalton Trans.*, 2017, **46**, 2524–2531.
 - 37 A. Kumar, S. Mondal, K. S. Kayshap, S. K. Hira, P. P. Manna, W. Dehaen and S. Dey, Water switched aggregation/disaggregation strategies of a coumarin-naphthalene conjugated sensor and its selectivity towards Cu²⁺ and Ag⁺ ions along with cell imaging studies on human osteosarcoma cells (U-2 OS), *New J. Chem.*, 2018, **42**, 10983–10988.
 - 38 C. Kumari, D. Sain, A. Kumar, H. P. Nayek, S. Debnath, P. Saha and S. Dey, A Non-Perilous Coumarin-Based Ratiometric Probe for 'In Vitro' Detection of Cu through Cell Imaging Technique, *ChemistrySelect*, 2017, **2**, 8270–8277.
 - 39 A. Kumar, D. Sain, C. Kumari and S. Dey, Detection of Hg²⁺ and Cs⁺ with a Rhodamine-based Sensor and Ethoxy-substituted Dihydroimidazole Ring Formation Associated with the Reduction of Hg²⁺ to Hg, *ChemistrySelect*, 2017, **2**, 1106–1110.
 - 40 C. Kumari, D. Sain, A. Kumar, H. P. Nayek, S. Debnath, P. Saha and S. Dey, A bis-hydrazone derivative of 2, 5-furandicarboxaldehyde with perfect hetero-atomic cavity for selective sensing of Hg(II) and its intracellular detection in living HeLa S3 cell, *Sens. Actuators, B*, 2017, **243**, 1181–1190.

- 41 I. T. Ho, K. C. Haung and W. S. Chung, 1, 3-Alternate Calix [4] arene as a Homobinuclear Ditopic Fluorescent Chemosensor for Ag⁺ Ions, *Chem. – Asian J.*, 2011, **6**, 2738–2746.
- 42 Y. H. Lau, P. J. Rutledge, M. Watkinson and M. H. Todd, Chemical sensors that incorporate click-derived triazoles, *Chem. Soc. Rev.*, 2011, **40**, 2848–2866.
- 43 E. Hao, T. Meng, M. Zhang, W. Pang, Y. Zhou and L. Jiao, Solvent dependent fluorescent properties of a 1, 2, 3-triazole linked 8-hydroxyquinoline chemosensor: tunable detection from Zinc(II) to Iron(III) in the CH₃CN/H₂O system, *J. Phys. Chem. A*, 2011, **115**, 8234–8241.
- 44 S. H. Kim, H. S. Choi, J. Kim, S. J. Lee, D. T. Quang and J. S. Kim, Novel optical/electrochemical selective 1, 2, 3-triazole ring-appended chemosensor for the Al³⁺ ion, *Org. Lett.*, 2009, **12**, 560–563.
- 45 S. Huang, R. J. Clark and L. Zhu, Highly sensitive fluorescent probes for zinc ion based on triazolyl-containing tetradentate coordination motifs, *Org. Lett.*, 2007, **9**, 4999–5002.
- 46 K. Sivakumar, F. Xie, B. M. Cash, S. Long, H. N. Barnhill and Q. Wang, A fluorogenic 1, 3-dipolar cycloaddition reaction of 3-azidocoumarins and acetylenes, *Org. Lett.*, 2004, **6**, 4603–4606.
- 47 W. Lin, L. Yuan, Z. Cao, Y. Feng and L. Long, A sensitive and selective fluorescent thiol probe in water based on the conjugate 1, 4-addition of thiols to α , β -unsaturated ketones, *Chem. – Eur. J.*, 2009, **15**, 5096–5103.
- 48 Y. Yang, T. Cheng, W. Zhu, Y. Xu and X. Qian, Highly selective and sensitive near-infrared fluorescent sensors for cadmium in aqueous solution, *Org. Lett.*, 2010, **13**, 264–267.
- 49 P.-T. Chou, G.-R. Wu, C.-Y. Wei, C.-C. Cheng, C.-P. Chang and F.-T. Hung, Excited-state amine–imine double proton transfer in 7-azaindoline, *J. Phys. Chem. B*, 2000, **104**, 7818–7829.
- 50 H. A. Benesi and J. Hildebrand, A spectrophotometric investigation of the interaction of iodine with aromatic hydrocarbons, *J. Am. Chem. Soc.*, 1949, **71**, 2703–2707.
- 51 S. N. Patil, F. Sanningannavar, B. Navati, D. Nagaraja, N. Patil and R. Melavanki, Quenching mechanism of 5BDTC by aniline using Stern–Volmer plots, *Can. J. Phys.*, 2015, **93**, 1076–1081.
- 52 M.-X. Liu, T.-B. Wei, Q. Lin and Y.-M. Zhang, A novel 5-mercapto triazole Schiff base as a selective chromogenic chemosensor for Cu²⁺, *Spectrochim. Acta, Part A*, 2011, **79**, 1837–1842.
- 53 C. Lee, W. Yang and R. G. Parr, Development of the Colle-Salvetti correlation-energy formula into a functional of the electron density, *Phys. Rev. B: Condens. Matter Mater. Phys.*, 1988, **37**, 785.
- 54 A. V. Titov, I. S. Ufimtsev, N. Luehr and T. J. Martinez, Generating efficient quantum chemistry codes for novel architectures, *J. Chem. Theory Comput.*, 2012, **9**, 213–221.
- 55 I. S. Ufimtsev and T. J. Martinez, Quantum chemistry on graphical processing units. 3. Analytical energy gradients, geometry optimization, and first principles molecular dynamics, *J. Chem. Theory Comput.*, 2009, **5**, 2619–2628.
- 56 N. Boens, V. Leen and W. Dehaen, Fluorescent indicators based on BODIPY, *Chem. Soc. Rev.*, 2012, **41**, 1130–1172.